HYDROGEN, FUEL CELL & ENERGY STORAGE

A sensorless adaptive non-linear control scheme for minimizing the stator energy losses of IPMSM

Mohammadreza Moradian[a,b,*] | **Jafar Soltani**[c] | **Hamid Ghorbani**[a]
Abbas Najar-khodabakhsh[a]

[a] Department of Electrical Engineering, Najafabad Branch, Islamic Azad University, Najafabad, Iran
[b] Smart Microgrid Research Center, Najafabad Branch, Islamic Azad University, Najafabad, Iran
[c] Faculty of Electrical and Computer Engineering, Isfahan University of Technology, Isfahan, Iran
[*] Corresponding author, Email: moradian@iaun.ac.ir

Article Information

Article Type
Research Article

Article History
Received: *20 Mar 2024*
Revised: *29 May 2024*
Accepted: *15 Jun 2024*
Published Online: *15 Jun 2024*

Keywords
Adaptive control
Input-output feedback linearization
IPMSM

Abstract

This study aims to investigate a direct torque and flux control scheme for an Interior Mounted Permanent Magnet Synchronous Motor (IPMSM) using an Adaptive Input-Output state Feedback-Linearization (AIOFL). In this control strategy, the rotor speed is evaluated basically by utilizing the momentary values of the enhanced electromagnetic torque and power. The generally stability of the drive system is demonstrated by Lyapunov hypothesis. For a given rotor reference speed and a rotor shaft load torque, the control strategy of Maximum Torque Per Ampere (MTPA) is performed by using a so-called stator flux search method. This search method is achieved by decreasing the magnitude of stator reference flux in small steps until the magnitude of stator current becomes minimum and as a result, the stator copper energy loss is minimized. The results of some computer simulations and tests, which have been came about, are displayed to demonstrate the viability and capability of the proposed control strategy.

Cite this article: Moradian, M., Soltani, J., Ghorbani, H., Najar-khodabakhsh, A., (2024). A sensorless adaptive non-linear control scheme for minimizing the stator energy losses of IPMSM. DOI: 10.22104/HFE.2024.6862.1295

DOI: 10.22104/HFE.2024.6862.1295

1 Introduction

Over the last two decades, the Interior Permanent Magnet Synchronous Motor (IPMSM) has been getting to be a great choice for industrial drive applications due to a few of its invaluable such as high power factor and power density, high torque to current proportion, high-energy effectiveness, large power to weight ratio and wide speed range of operating [1–4].

Commonly used Direct Torque and flux Control (DTC) of IPMSM based on utilizing the bang-bang or hysteresis controllers have been examined since the 1990s, in which the exact information of the stator resistance especially within the rotor low-speed operation is required [5]. In spite of the fact that such strategy is straightforward, it has a few shortcomings including acoustic noise, high torque and flux fluctuations, and dependency of switching frequency to the speed, the load torque and the chosen hysteresis bands. In [6–8] a direct flux vector control strategy utilizing one proportional-integral (PI) controller and space vector modulation (SVM) with constant switching frequency and minor torque ripple has been presented.

Xu et al. [9] proposed a direct torque control scheme using the variable structure approach. This scheme reduces the flux and torque ripples noticeably but is very complicate and parameter dependent.

A DTC method has been described in [10] that is based on adaptive state feedback linearization, the compact parameters estimated by Lyapunov theory which have no relation to those of need to use in the control input function obtained by the same theory. This means that according to [10], in order to determine the reference motor drive voltage, the corresponding rated values of parameters of L_d, L_q and R_s has been considered. As a result, the overall stability of the drive system can never be guaranteed with subject to motor parameters uncertainties and load disturbances.

The Maximum Torque-Per-Ampere (MTPA) technique for IPMSM drives is a parameter subordinate strategy [11,12]. The saturation influences the *d*-*q* axis inductances, so that online or offline parameter recognizing is essential to perform the MPTA. In off-line parameter distinguishing, IPMSM electrical parameters are determined in accordance to a specific load point by experiments and embedded into the reference tables or numerically inexact by specific curves. Online parameter evaluation strategies as the Recursive Least Squares (RLS), and Expanded Kalman Filter (EKF), techniques are mathematically severe as they include matrix operations [13–17].

For sensorless IPMSM speed drive, in [18] a sliding mode standard observer for a MTPA based control strategy is described to detect the position of the rotor. Accordingly, the required *d*-*q* axis stator current for MTPA is obtained by the means of a special method, in which a PI rotor speed controller is utilized to determine the corresponding motor reference current amplitude for MTPA strategy which is seriously dubious. In fact, MTPA control method of any ac drive system means that for a desire motor electromagnetic torque upon a desire rotor speed, the ratio of torque per ampere should be minimum. Unfortunately this important point has been confused in [18], since in that study to get MTPA point, it has been tried to make the electromagnetic torque maximum and simultaneously the motor current minimum. In [18], Fast Fourier Transform (FFT) method is used to detect the on-line sampled dc components of the motor d and q axis currents. Such methods generate some delays and phase shifts which make the motor dynamic system slow. In addition, it can cause the motor closed loop system control becomes unstable.

In [19], according to MTPA control strategy, the motor's *d*-*q* current references would be accessible by Fuzzy-Logic Controller (FLC). The motor torque reference can be calculated by means of the nominal values of the inductance, it is essential for efficiency enhancement. The presented strategy in [19] would result in some short comes as:

- The FLC controller permits the machine direct axis currents to be positive which is not suitable in IPMSM drive.
- The control strategy is not stable and robust with subject to machine parameters uncertainties and disturbances. It is reminding that in [19] the machine nominal parameters have been used.
- For each chosen machine, at the first stage some tests are required to be performed in order to obtain the motor equivalent iron loss resistance (Rc) curves versus motor speed variation. This procedure makes the proposed method time consuming and troublesome.

Current minimizing torque control of IPMSM utilizing Ferrari's strategy is explained in [20]. This strategy gives the solution to a quartic equation for the torque control. The major shortcoming of the explained strategy is that, due to impacts of the magnetic saturation on the machine *d*-*q* axis variables, the look-up tables and curves have to be off-line rehashed. Moreover, the calculations utilized within the proposed strategy are truly complicate and time expending.

Sensorless control methodology of IPMSM drives may be classified into two classes:

- Spatial saliency image tracking strategies utilizing the injection of high-frequency (HF) signals plus the fundamental [21,22],

- Strategies utilizing electromotive force (EMF) evaluation with fundamental excitation [23].

The strategies of injecting signal are on the basis of identifying the saliency or the magnetic saturation which resulted in structural anisotropy and the rotor speed and the corresponding EMF of the IPMSM. Whereas, each method has its benefits and confinements. The impacting components incorporate the constrained precision of estimations, parameter variation of the motor, and presence of the inverter nonlinearities or create more acoustic noise and losses.

Among the efficient nonlinear control methods, it can be referred to our previous research described in [24–26]. It is worthwhile mentioning that the present research is a continuation of our previous research that has been presented in [26].

In this study, an Adaptive Input-Output state Feedback-Linearization (AIOFL) control methodology is designed for DTC of IPMSM drives. Speed of the rotor is detected online by a very simple observer which operates in parallel with drive system controller. In accordance to the Lyapunov theory, the overall stability of the proposed scheme is proved. Using a so-called simple method based on on-line searching the magnitude of the squared of the stator flux, the control strategy of MTPA corresponding to IPMSM drive is implemented. The explained strategy of this study is validated by sufficient computer simulations and practical tests.

2 Modeling an IPMSM

Alluding to [27], the d-q axis equations related to the IPMSM can be written as:

$$v_{qs} = R_s\, i_{qs} + \frac{d\lambda_{qs}}{dt} + \omega_{re}\lambda_{ds}\,, \tag{1}$$

$$v_{ds} = R_s\, i_{ds} + \frac{d\lambda_{ds}}{dt} - \omega_{re}\lambda_{qs}\,, \tag{2}$$

with

$$\begin{cases} \lambda_{ds} = L_d\, i_{ds} + \lambda_m\,, \\ \lambda_{qs} = L_q\, i_{qs}\,, \end{cases} \tag{3}$$

where the d-q axis stator fluxes linkage, voltage, currents and inductances are λ_{ds}, λ_{qs}, v_{ds}, v_{qs}, i_{ds}, i_{qs}, L_{ds} and L_{qs}, respectively. R_s, λ_m and ω_{re} are the stator resistance, PM flux linkage and the electrical angular speed of the rotor.

Also, the electromagnetic generated torque of the mentioned drive is given by [28]:

$$T_e = \frac{3P}{2}\left(\lambda_{ds} i_{qs} - \lambda_{qs} i_{ds}\right), \tag{4}$$

where the number of rotor pole pairs is displayed by P. Additionally, in terms of mechanical equation, one can get:

$$J_r\,\frac{d\omega_r}{dt} = P(T_e - T_l) - B_r\omega_r\,, \tag{5}$$

where the moment inertia of the rotor is J_r. Considering B_r as the friction coefficient, ω_r as rotor mechanical angular speed and torque constant K_l, $T_l = K_l\omega_r$ which T_l denotes the motor load torque.

3 Input-output feedback Linearization

An Input-Output Feedback Linearization (IOFL) method, which is a nonlinear control technique adopted for nonlinear plants, is utilized in this study in order to directly control torque and stator flux of an IPMSM drive system as the objective function. Based on Equations (1) to (5):

$$\dot{X} = f(X) + g(X)\,U\,, \tag{6}$$

with

$$X = \begin{bmatrix} x_1 & x_2 & x_3 \end{bmatrix}^T = \begin{bmatrix} \lambda_{qs} & \lambda_{ds} & \omega_{re} \end{bmatrix}^T, \tag{7}$$

$$f(X)=\begin{bmatrix} f_1 \\ f_2 \\ f_3 \end{bmatrix},\ g(X)=\begin{bmatrix} g_1 & g_2 \end{bmatrix}=\begin{bmatrix} 1 & 0 \\ 0 & 1 \\ 0 & 0 \end{bmatrix},\ U=\begin{bmatrix} v_{qs} \\ v_{ds} \end{bmatrix}$$

$$f_1 = -R_s\,\frac{\lambda_{qs}}{L_q} - \omega_{re}\lambda_{ds}\,, \tag{8}$$

$$f_2 = -R_s\,\frac{\lambda_{ds}-\lambda_m}{L_d} + \omega_{re}\lambda_{qs}\,, \tag{9}$$

$$f_3 = \left[\frac{3P}{2J_r}\left\{\frac{L_d-L_q}{L_dL_q}\,\lambda_{qs}\,\lambda_{ds} + \frac{\lambda_{ds}}{L_d}\,\lambda_m\right\} - \frac{T_l}{J_r}\right]\Big/\left(\frac{P}{2}\right) - \frac{B_r}{J_r}\omega_{re}\,. \tag{10}$$

The output parameters can be introduced as:

$$y_1 = \lambda_s^2 = \lambda_{ds}^2 + \lambda_{qs}^2\,, \tag{11}$$

$$y_2 = T_e = \frac{3P}{2}\left[\lambda_{ds}\,\frac{\lambda_{qs}}{L_q} - \lambda_{qs}\,\frac{\lambda_{ds}-\lambda_m}{L_d}\right]. \tag{12}$$

Using Lie derivative theory [28], one can get:

$$\begin{bmatrix} \dot{y}_1 \\ \dot{y}_2 \end{bmatrix} = \begin{bmatrix} L_f y_1 \\ L_f y_2 \end{bmatrix} + \begin{bmatrix} L_{g1}y_1 & L_{g2}y_1 \\ L_{g1}y_2 & L_{g2}y_2 \end{bmatrix} \begin{bmatrix} u_1 \\ u_2 \end{bmatrix} \tag{13}$$

with

$$L_f y_1 = L_{11}\,\frac{1}{L_q} + L_{12}\,\frac{1}{L_d}\,, \tag{14}$$

$$L_f y_2 = L_{21}\,\frac{1}{L_q} + L_{22}\,\frac{1}{L_d}\,, \tag{15}$$

$$\begin{bmatrix} u_1 \\ u_2 \end{bmatrix} = \begin{bmatrix} v_{qs} \\ v_{ds} \end{bmatrix} \tag{16}$$

where L_{11}, L_{12}, L_{21}, L_{22}, $L_{g1}y_1$, $L_{g1}y_2$, $L_{g2}y_1$ and $L_{g2}y_2$ has been introduced in the Appendix A.

Assuming the drive system, dynamic errors are defined by:

$$\begin{cases} e_1 = \lambda_s^2 - \lambda_s^{*2} \\ e_2 = T_e - T_e^* \end{cases} \tag{17}$$

where the reference value is denoted by "$*$". By Combining Equations (17) and (13), the dynamic error can be rewritten as:

$$\begin{aligned} \begin{bmatrix} \dot{e}_1 \\ \dot{e}_2 \end{bmatrix} &= \begin{bmatrix} L_{11} & L_{12} \\ L_{21} & L_{22} \end{bmatrix} \begin{bmatrix} \theta_1 \\ \theta_2 \end{bmatrix} \\ &+ \begin{bmatrix} L_{g1}y_1 & L_{g2}y_1 \\ L_{g1}y_2 & L_{g2}y_2 \end{bmatrix} \begin{bmatrix} u_1 \\ u_2 \end{bmatrix} - \begin{bmatrix} (\lambda_s^{*2})' \\ (T_e^{*2})' \end{bmatrix}, \\ \theta = \begin{bmatrix} \theta_1 & \theta_2 \end{bmatrix}^T &= \begin{bmatrix} \dfrac{1}{L_q} & \dfrac{1}{L_d} \end{bmatrix}^T. \end{aligned} \tag{18}$$

Considering vector θ to be a known consistent vector, utilizing IOFL technique [29], the corresponding efforts of the system can be given as

$$\begin{bmatrix} u_1 \\ u_2 \end{bmatrix} = \begin{bmatrix} L_{g1}y_1 & L_{g2}y_1 \\ L_{g1}y_2 & L_{g2}y_2 \end{bmatrix}^{-1} \begin{bmatrix} \dot{y}_1^* - L_f y_1 - \alpha_1 e_1 \\ \dot{y}_2^* - L_f y_2 - \alpha_2 e_2 \end{bmatrix}. \tag{19}$$

Substituting Equation (19) in Equation (18), gives:

$$\begin{cases} \dfrac{de_1}{dt} = -\alpha_1 e_1 \,, \\ \dfrac{de_2}{dt} = -\alpha_2 e_2 \,, \end{cases} \tag{20}$$

where optional positive constants (α_1, α_2) drive Equation (20) exponentially meet to zero.

4 AIOFL

Since the machine parameters are uncertain, it is required to on-line estimate of vector θ given in Equation (18). Moreover, a precise evaluation of the stator resistance is additionally essential to measure the stator flux components within the (DS-QS) stationary reference frame. For this point, an observer is utilized and described in the section 5. Supplanting the evaluated vector $\hat{\theta}$ in Equation (18), comes about in

$$\begin{aligned} \begin{bmatrix} \dot{e}_1 \\ \dot{e}_2 \end{bmatrix} &= \begin{bmatrix} L_{11} & L_{12} \\ L_{21} & L_{22} \end{bmatrix} \begin{bmatrix} \hat{\theta}_1 \\ \hat{\theta}_2 \end{bmatrix} \\ &+ \begin{bmatrix} L_{g1}y_1 & L_{g2}y_1 \\ L_{g1}y_2 & L_{g2}y_2 \end{bmatrix} \begin{bmatrix} u_1 \\ u_2 \end{bmatrix} - \begin{bmatrix} (\dot{\lambda}_s^{*2})' \\ (\dot{T}_e^{*2})' \end{bmatrix}. \end{aligned} \tag{21}$$

Consequently Equations (18), (20) and (21) will be:

$$\dot{e} = -\alpha e + g(X)(\theta - \hat{\theta})\,, \tag{22}$$

$$\hat{\theta} = \begin{bmatrix} \hat{\dfrac{1}{L_q}} & \hat{\dfrac{1}{L_d}} \end{bmatrix}^T, \tag{23}$$

$$e = \begin{bmatrix} e_1 & e_2 \end{bmatrix}, \alpha = \begin{bmatrix} \alpha_1 & 0 \\ 0 & \alpha_2 \end{bmatrix}, \alpha_1, \alpha_2 > 0 \tag{24}$$

$$g(X) = \begin{bmatrix} g_{11}(x) & g_{12}(x) \\ g_{21}(x) & g_{22}(x) \end{bmatrix}, \tag{25}$$

where

$$g_{11}(x) = -2\lambda_{qs}^2 \hat{R}_s\,, \tag{26}$$

$$g_{12}(x) = -2\lambda_{ds}^2 \hat{R}_s + 2\lambda_{ds}\hat{R}_s\lambda_m\,, \tag{27}$$

$$\begin{aligned} g_{21}(x) = \frac{3P}{2}\big[&- \lambda_{ds}\hat{R}_s i_{qs} + \omega_{re}(\lambda_{qs}^2 - \lambda_{ds}^2) \\ &+ \lambda_{ds} v_{qs}\big]\,, \end{aligned} \tag{28}$$

$$\begin{aligned} g_{22}(x) = \frac{3P}{2}\big[&- \omega_{re}\lambda_{ds}\lambda_m + \lambda_{qs}\hat{R}_s i_{ds} \\ &+ \omega_{re}(\lambda_{re}^2 - \lambda_{qs}^2) - \lambda_{qs} v_{ds}\big]\,. \end{aligned} \tag{29}$$

Equation (22) can be written as:

$$\begin{aligned} \dot{x} &= Ax + W^T\tilde{\theta}\,, \\ x &= \begin{bmatrix} e_1 & e_2 \end{bmatrix}^T, \ \tilde{\theta} = \begin{bmatrix} \tilde{\theta}_1 & \tilde{\theta}_2 \end{bmatrix}^T, \\ A &= \begin{bmatrix} -\alpha_1 & 0 \\ 0 & -\alpha_2 \end{bmatrix}, \ W^T = \begin{bmatrix} g_{11}(x) & g_{12}(x) \\ g_{21}(x) & g_{22}(x) \end{bmatrix}. \end{aligned} \tag{30}$$

The Lyapunov function is considered as below:

$$\begin{aligned} V &= \frac{1}{2}x^T x + \frac{1}{2}\tilde{\theta}^T \Gamma^{-1}\tilde{\theta}\,, \\ \Gamma &= \mathrm{diag}[\gamma_1, \gamma_2]^T\,, \end{aligned} \tag{31}$$

where the positive gains of adaption are γ_1 and γ_2.

According to the derived V with regard to time (sec) comes about in [24]:

$$\dot{V} = \frac{1}{2}\dot{x}^T x + \frac{1}{2}x^T\dot{x} + \frac{1}{2}\dot{\tilde{\theta}}^T \Gamma^{-1}\tilde{\theta} + \frac{1}{2}\tilde{\theta}^T \Gamma^{-1}\dot{\tilde{\theta}}\,. \tag{32}$$

Substituting $\dot{x}$ from Equation (30) into Equation (32) yields [12]:

$$\dot{V} = x^T A\, x + \tilde{\theta}^T W x + \tilde{\theta}^T \Gamma^{-1}\dot{\tilde{\theta}}\,. \tag{33}$$

Assuming the following adaption law:

$$\tilde{\theta}^T W x + \tilde{\theta}^T \Gamma^{-1}\dot{\tilde{\theta}} = 0\,, \quad \dot{\tilde{\theta}} = -\Gamma W x\,, \tag{34}$$

then, Equation (32) is reduced to:

$$\dot{V} = x^T A\, x\,. \tag{35}$$

Because $A < 0$, hence from Equation (35),

$$\dot{V} \leq 0 \,. \tag{36}$$

$1/L_d$ and $1/L_q$ are assumed to be unknown constant parameters, hence,

$$\dot{\tilde{\theta}}_1 = -\dot{\hat{\theta}}_1 \,, \quad \dot{\tilde{\theta}}_2 = -\dot{\hat{\theta}}_2 \,. \tag{37}$$

As a result, from Equation (34), the adaption laws are obtained as:

$$\begin{bmatrix} \dot{\hat{a}}_1 \\ \dot{\hat{a}}_2 \end{bmatrix} = -\begin{bmatrix} -\gamma_1 & 0 \\ 0 & -\gamma_2 \end{bmatrix} \begin{bmatrix} g_{11}(x) & g_{12}(x) \\ g_{21}(x) & g_{22}(x) \end{bmatrix} \begin{bmatrix} e_1 \\ e_2 \end{bmatrix} \,. \tag{38}$$

5 Stator resistance estimation

Figure 1 demonstrates the field oriented reference frame (x, y) of the IPMSM stator flux control.

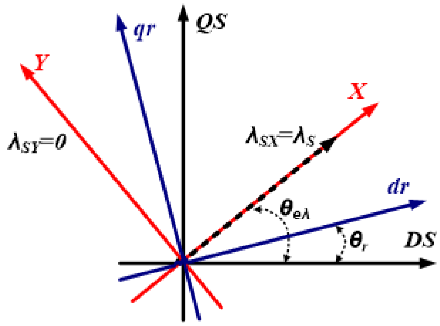

Fig. 1. IPMSM reference frames.

In this reference frame, the machine electromagnetic generated torque is obtained as:

$$T_e = \frac{3P}{2} \lambda_{sx}\, i_{sy} \tag{39}$$

Referring to Figure 2, the output of rotor speed PI controller is T_e^*.

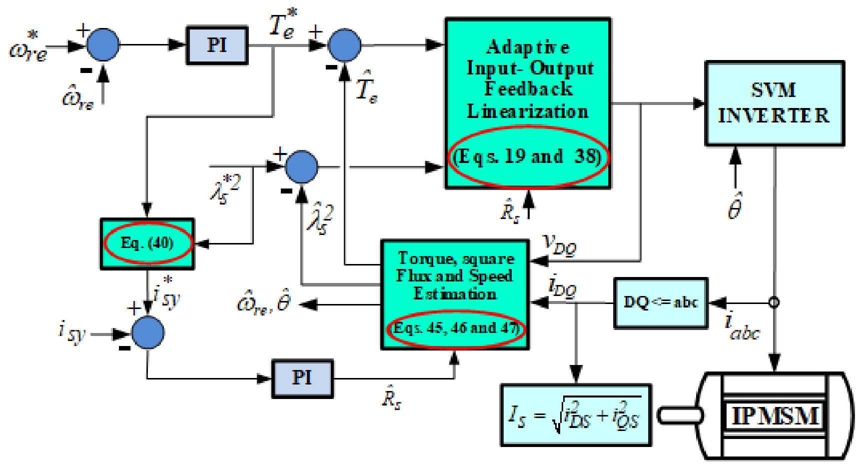

Fig. 2. Drive system control block diagram for an IPMSM.

As a result, using Equation (39), assuming $\lambda_{sx} = \lambda_s^*$, the y-axis stator reference current can be obtained as:

$$i_{sy}^* = \frac{T_e^*}{\frac{3}{2} P \lambda_s^*} \tag{40}$$

An additional PI controller is used to estimate the stator resistance as shown in Figure 2.

6 Voltage sensors dismissal

An effective way to exclude the dc offset caused by voltage sensors is the estimation of the phase voltages based on the state of switching inverter (S_a, S_b, S_c) and dc-link voltage [30]. While, practically, our switching patterns are applied to the PWM inverter by means of the Complex Programmable Logic Device (CPLD) with 1 μs resolution. To address this issue, the average phase voltages in each sampling interval (5 kHz) are calculated utilizing the segment number of reference voltage space vector and timing task of SVM-PWM inverter which is accessible by the PC. The status of upper switch of each leg is reported in Table 1, considering the inverter reference voltage vector which is found in accordance to the number of sector. S_a, S_b, and S_c advert to upper switch status of a, b and c phases, respectively. Referring to Table 1, the inverter's average phase voltages within a sampling of T_s, is gotten as

$$\begin{pmatrix} v_{aN} \\ v_{bN} \\ v_{cN} \end{pmatrix} = \frac{V_{\mathrm{DC}}}{T_s} S_{\mathrm{eci}} \begin{pmatrix} t_1 \\ t_2 \end{pmatrix} \,, \tag{41}$$
$$i = [1, \ldots, 6] \,, \quad T_s = t_0 + t_1 + t_2 \,,$$

Table 1. Status of inverter leg upper switch according to sector number.

Sector No.	1		2		3		4		5		6	
	t_1	t_2	t_1	t_2	t_1	t_2	t_1	t_2	t_1	t_2	t_1	t_2
S_a	1	1	1	0	0	0	0	0	0	1	1	1
S_b	0	1	1	1	1	1	1	0	0	0	0	0
S_c	0	0	0	0	0	0	1	1	1	1	1	0

where DC link voltage is V_{DC} with negative polarity as N. t_1 and t_2 are the timing task and S_{eci} is i^{th} sector matrix which is gotten from Table 1.

Obviously, the components of space voltage in two-axis stationary reference frame can be gotten as [31]:

$$v_{DS} = \frac{2}{3}(v_{aN} - 0.5v_{bN} - 0.5v_{cN})\,, \tag{42}$$

$$v_{QS} = \frac{1}{\sqrt{3}}(v_{bN} - v_{cN})\,. \tag{43}$$

Due to ineffectiveness of the t_0 on the space vector of stator voltage (v_{DS}, v_{QS}), the Table 1 is not contained with the status reports of the upper switch of each inverter leg.

7 IPMSM rotor-speed estimation

A simple method is used for on-line detecting of the rotor speed which is described as follows.

The IPMSM electromagnetic or airgap real power is described by [24]:

$$P_g = \frac{3}{2}(v_{DS}\, i_{DS} + v_{QS}\, i_{QS}) - \frac{3}{2}\hat{R}_s(i_{DS}^2 + i_{QS}^2)\,, \tag{44}$$

where the d-q axis stator currents in the stationary reference frame are i_{DS} and i_{QS}, respectively.

The electromagnetic torque (T_{em}) is estimated as

$$T_{em} = \frac{3P}{2}(\lambda_{DS}\, i_{QS} - \lambda_{QS}\, i_{DS})\,, \tag{45}$$

where λ_{DS} and λ_{QS} are D-Q axis stator fluxes linkage with respect to stationary reference frame.

$$\begin{aligned} \lambda_{DS} &= \int (v_{DS} - \hat{R}_s\, i_{DS})\, dt \\ \lambda_{QS} &= \int (v_{QS} - \hat{R}_s\, i_{QS})\, dt \end{aligned} \tag{46}$$

From Equations (44) and (45), having estimated the real values of the motor electromagnetic torque (T_{em}), and the motor airgap power (P_g), the rotor speed is obtained by

$$\hat{\omega}_m = \frac{P_g}{T_{em}} \tag{47}$$

The estimated speed by Equation (47) has some harmonics due to using the rotor airgap power and electromagnetic torque. To eliminate these harmonics a simple low pass filter is employed as:

$$\hat{\omega}_{mf} = \frac{\omega_c\, \hat{\omega}_m}{p + \omega_c} \tag{48}$$

where p denotes d/dt, $\omega_c = 2\pi f_c$ and $f_c = 10\,\mathrm{Hz}$ is cutoff frequency of the mentioned filter.

8 IPMSM MTPA control strategy

As illustrated in Figure 2, in order to online detection of the electromagnetic reference torque of the motor (T_e^*), a conventionally known PI controller is used. For a desire rotor speed (ω_{re}^*) and a given rotor shaft torque, the squared of the stator flux reference (λ_s^{*2}) is decreased in steps until the amplitude of the stator current determined by $I_s = (i_{DS}^2 + i_{QS}^2)^{0.5}$ reaches to its minimum value. It should be noted that small steps have to be chosen for decreasing the stator flux such that at the end of each step, the steady-state condition is to be reached. Having done that, the amplitude of stator current corresponding to each step is saved. This procedure is repeated until the minimum value of the stator current is to be obtained.

9 Simulation and experimental results

9.1 Simulation results

Referring to the described IOFL in former sections, Figure 2 displays the general view of the DTC and stator flux control of an IPMSM drive system. A C++ script has been modified for simulation of the system outlined in Figure 2. For the proposed IPMSM in Table 2, some simulation results are depicted in Figures 3 to 7. According to the described practical test in subsequent section, the two axis reactances of this motor have been determined. The corresponding control gains of the drive system is obtained by trial and error: K_P, K_I, γ_1 and $\alpha_1 = \alpha_2$ equal to 0.05, 0.15, 0.4, 0.8 and 250 respectively.

Table 2. Parameters of the IPMSM.

Num. rotor pole pairs	P	2
Resistance of stator	R	$21.1\,\Omega$
PM flux linkage	λ_m	0.493 Wb
Rated d-axis inductance	L_d	0.3 H
Rated q-axis inductance	L_q	0.8 H
Phase voltage	V_s	155 V
Peak/RMS phase current	I_s	1.1 A
Frequency	f	50 Hz
Rated torque	T_n	2.2 Nm
Rated power	P_n	370 W
Equivalent rotor inertia	J_r	$0.00045\,\mathrm{kg \cdot m^2}$
Viscous friction coefficient	B_r	$0.00174\,\mathrm{N \cdot m \cdot s/rad}$
Torque constant	K_l	$0.012\,\mathrm{N \cdot m \cdot s/rad}$

In terms of an exponential rotor reference, speed rising from 0 to 125.6 Elec · rad/s upon $\tau = 1\,$s rise time, steps down/up the stator reference flux (λ_s^{*2}) from 0.465 to 0.4 Wb^2 at $t = 10\,$s, and from 0.4 to 0.52 Wb^2 at $t = 12.5\,$s. In the end, the rotor reference speed is exponentially expanding from 125.6 to 157 Elec · rad/s with $\tau = 0.25\,$s rise time at $t = 17.5\,$s. Considering an exponential rotor reference speed rising from zero to 157 rad/s upon $\tau = 1\,$s rise time and $\lambda_s^{*2} = 0.465\,\mathrm{Wb}^2$, the steady-state situation is gotten to begin with for this test, at that point utilizing the MTPA control strategy depicted in section 8. Figures 3 to 7 display the corresponding results for the clarified tests.

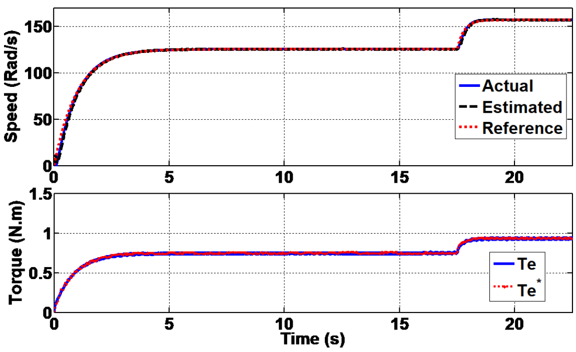

Fig. 3. Simulation results of torque and speed of IPMSM drive.

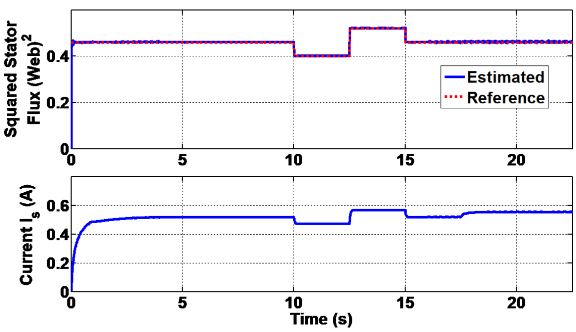

Fig. 4. Simulation results of squared of the stator flux and current amplitude of IPMSM drive.

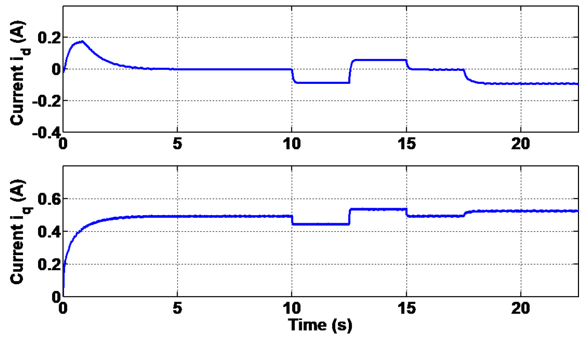

Fig. 5. Simulation results of d- and q-axes currents of IPMSM drive.

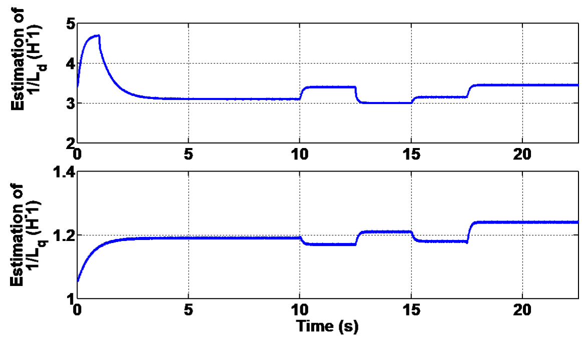

Fig. 6. Simulation results of $\frac{1}{\hat{L}_d}$ and $\frac{1}{\hat{L}_q}$ estimation.

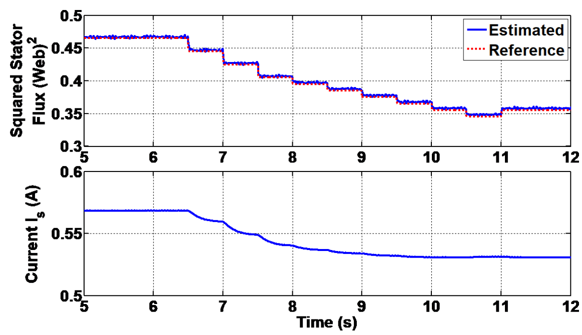

Fig. 7. Simulation results of MTPA strategy of IPMSM drive.

9.2 Experimental results

9.2.1 Practical system setup

In terms of real-world performance assessment of the proposed system, a PC-based experimental set up was adopted (Figure 8), based on the general block diagram in Figure 2 in which a personal computer (PC) was considered with the following parts, in order to calculate the evaluated signals and display the registered waveforms:

i. **Motor:** a 0.5 hp 3-P IPMSM;
ii. **Load:** a 0.5 kW DC generator;

iii. **Supply:** 3-P Voltage Source Inverter (VSI) plus required isolations board;
iv. **Sensors:** sensor boards for voltage and current measurement;
v. **IO card:** Advantech digital Input-Output card (48 bit);
vi. **A/D card:** Advantech A/D converter (32-channel);
vii. **CPLD board**.

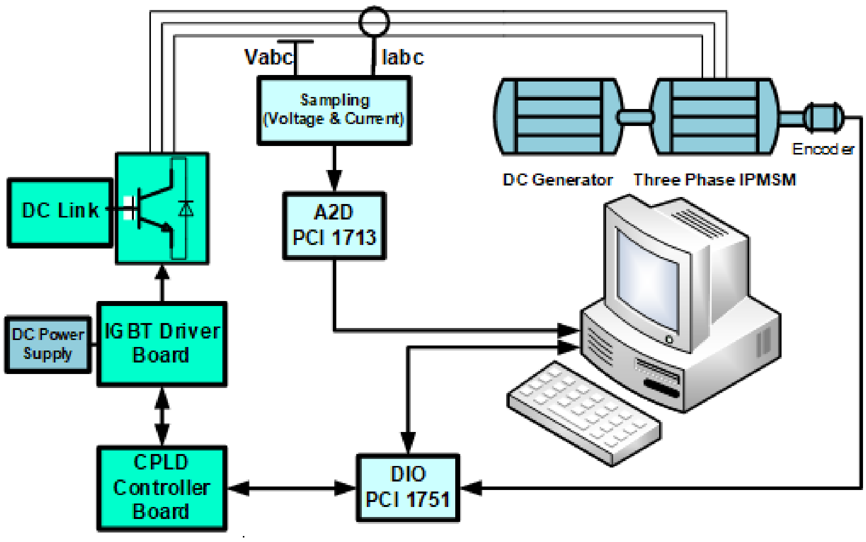

Fig. 8. Laboratory implementation block diagram.

A 3-P inverter which benefits from two level symmetrical space vector modulation (SVM) is applied for system supply. In order to implement switching patterns, a CPLD (EPM240T100) with the switching frequency up to 5 kHz is selected, which PC communicates accomplished through PCI-1751 (Advantech Digital I/O board). Generating corresponding SVM-based switching patterns for IGBT switches and then providing the required best dead time for power switches, providing PC-hardware synchronization signal for data transmission and considering inverter shutdown statues caused by over-current or hardware hanging states are the realized tasks of the CPLD. Hall-type LEM sensors are applied for dc-link voltage and phase currents measurements. The evaluated electrical signals are passed through an analog separated 2$^{\text{nd}}$ order low pass filter (LPF bandwidth: 1.5 kHz). At that point, digital signals are produced by utilizing of a 10 μs conversion time A/D card.

To assess the exactness of the rotor-speed and position, the genuine position of the rotor is gotten from an utter encoder with 1024 pulses/r. This laboratory setup is shown in Figure 9.

9.2.2 Measuring L_d and L_q

Firstly, the d-q axis voltages and currents ((v^r_{qs}, v^r_{ds}) and (i^r_{qs}, i^r_{ds}), respectively) were measured by means of considered sensors. Afterwards, dc components of the measured values were excluded using a 1$^{\text{st}}$ order LPF.

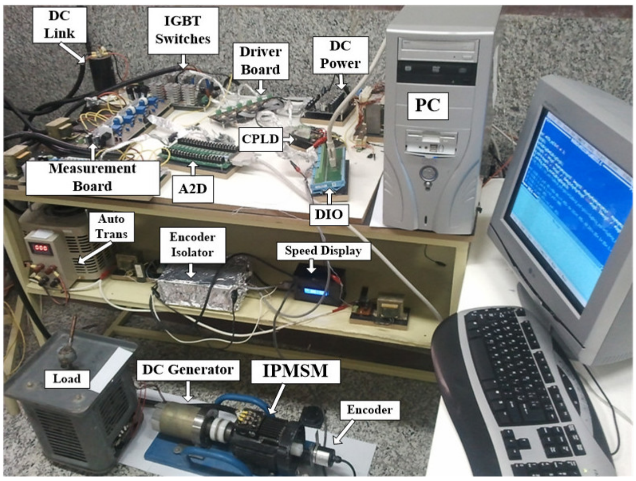

Fig. 9. Experimental setup.

Considering described voltage Equations (1) and (2), the corresponding d-q axis inductances of the proposed drive for steady state condition can be given as:

$$\lambda_{ds} = \frac{v_{qs} - R_s i_{qs}}{\omega_{re}}, \quad \lambda_{qs} = \frac{v_{ds} - R_s i_{ds}}{-\omega_{re}}, \tag{49}$$

$$L_{ds} = \frac{\lambda_{ds} - \lambda_m}{i_{ds}}, \quad L_{qs} = \frac{\lambda_{qs}}{i_{qs}}. \tag{50}$$

With regard to unnecessity of knowing the accurate value of *d*-*q* axis inductances for the proposed control strategy in this study, in order to determine such parameters, an open loop control was performed practically at rated currents and speed of the IPMSM.

9.2.3 Experimental test

Figures 10 to 13 illustrate the experimental results using operational conditions similar to the performed simulations. Accordingly, a good agreement is achieved, in comparison with the simulated results (Figures 3 to 6).

Figure 14 exhibits the experimental results, applying MTPA control strategy. In comparison with the simulated results shown in Figure 7, the practical results are also in a good agreement.

10 Conclusion

The goal of this study is to develop an IO feedback linearization control scheme (AIOFL) in order to directly drive speed (torque) and the squared of the stator flux in an IPMSM. The overall stability of this control method has been proved by Lyapunov theory. Considering instant values of motor torque and power and by means of a simple 1st order low pass filter, the rotor speed is obtained in this control scheme. In addition to the proposed AIOFL method, an IPMSM drive system was implemented by a practical setup and test and computer simulation were operated for a 0.5 hp (0.37 kW) IPMSM.

The results exceptionally well affirm the legitimacy and viability of the proposed control technique in this research. A so-called stator flux search method was applied to accomplish the MTPA control scheme for the IPMSM. Again, a good agreement exists between simulation and experimental results obtained for this test. It should be mentioned that the accurate value of the initial rotor position is needed for implementation of both the tests described in this study. In comparison with the control methods, presented in previous research, in order to apply the proposed control strategy, the knowledge of the actual values of the motor *d*-*q* axis inductances is not essential.

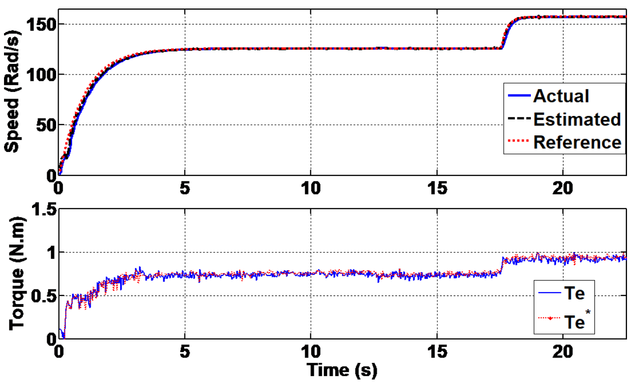

Fig. 10. Torque and speed of IPMSM drive.

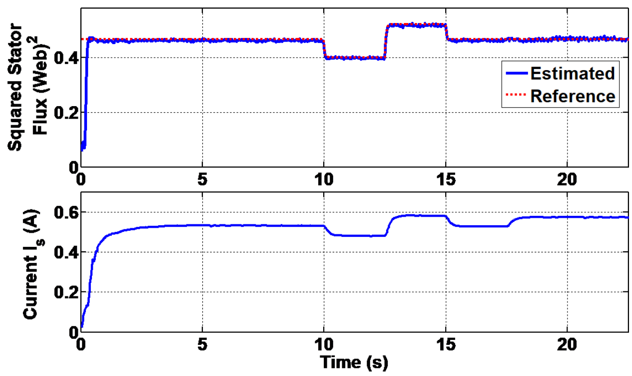

Fig. 11. Squared stator flux and current amplitude of IPMSM drive.

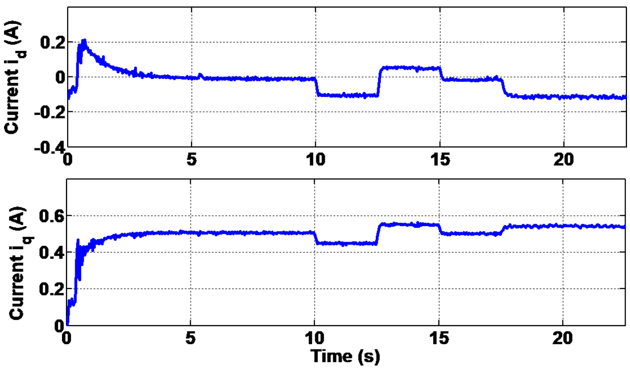

Fig. 12. *d*- and *q*-axes currents of IPMSM drive.

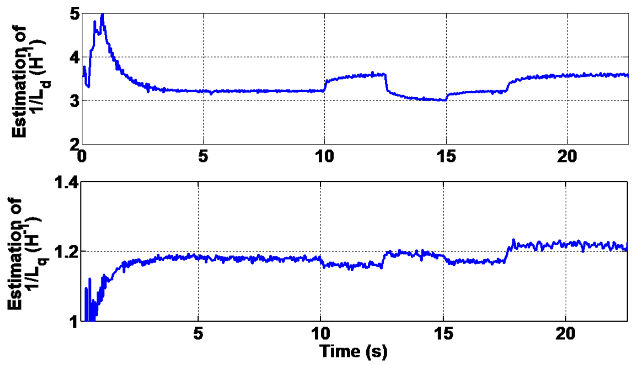

Fig. 13. Estimation of $\frac{1}{\hat{L}_d}$ and $\frac{1}{\hat{L}_q}$.

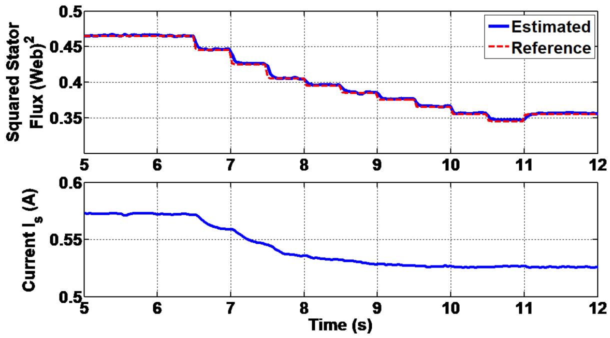

Fig. 14. Experimental results of MTPA strategy of IPMSM drive.

A Appendix

$$
\begin{aligned}
L_{11} &= -2\lambda_{qs}^2 R_s\,,\\
L_{12} &= -2\lambda_{ds}^2 R_s + 2\lambda_{ds}R_s\lambda_m\,,\\
L_{21} &= \frac{3P}{2}\big[-\lambda_{ds}R_s i_{qs} + \omega_{re}(\lambda_{qs}^2 - \lambda_{ds}^2)\big]\,,\\
L_{22} &= \frac{3P}{2}\big[-\omega_{re}\lambda_{ds}\lambda_m + \lambda_{qs}R_s i_{ds} + \omega_{re}(\lambda_{ds}^2 - \lambda_{qs})\big]\,,\\
L_{g1}y_1 &= 2\lambda_{qs}\,,\\
L_{g2}y_1 &= 2\lambda_{ds}\,,\\
L_{g1}y_2 &= \frac{3P}{2}\Big(\frac{\lambda_{ds}}{L_q} - i_{ds}\Big)\,,\\
L_{g2}y_2 &= \frac{3P}{2}\Big(i_{qs} - \frac{\lambda_{qs}}{L_d}\Big)\,.
\end{aligned}
$$

References

[1] Li X, Dai C, Chen W, Geng Q, Wang H. Position Detection and Speed Recording Method for Power-off IPMSM in Full-Speed Range Based on Ultrahigh Frequency Signal Injection. IEEE Transactions on Power Electronics. 2023;. 132

[2] Wang Z, Yu K, Li Y, Gu M. Position sensorless control of dual three-phase IPMSM drives with high-frequency square-wave voltage injection. IEEE Transactions on Industrial Electronics. 2022;70(10):9925–9934. 132

[3] Choi CH, Seok JK, Lorenz RD. Wide-speed direct torque and flux control for interior PM synchronous motors operating at voltage and current limits. IEEE Transactions on Industry Applications. 2012;49(1):109–117. 132

[4] Yoo J, Kim HS, Sul SK. MTPA tracking control of sensorless IPMSM based on square-wave voltage signal injection. IEEE Transactions on Power Electronics. 2022;37(10):12525–12537. 132

[5] Rahman MF, Zhong L, Lim KW. A direct torque-controlled interior permanent magnet synchronous motor drive incorporating field weakening. IEEE Transactions on Industry Applications. 1998;34(6):1246–1253. 132

[6] Tang L, Zhong L, Rahman MF, Hu Y. A novel direct torque control for interior permanent-magnet synchronous machine drive with low ripple in torque and flux-a speed-sensorless approach. IEEE Transactions on industry applications. 2003;39(6):1748–1756. 132

[7] Tang L, Zhong L, Rahman MF, Hu Y. A novel direct torque controlled interior permanent magnet synchronous machine drive with low ripple in flux and torque and fixed switching frequency. IEEE Transactions on power electronics. 2004;19(2):346–354. 132

[8] Inoue Y, Morimoto S, Sanada M. Examination and linearization of torque control system for direct torque controlled IPMSM. IEEE Transactions on Industry Applications. 2009;46(1):159–166. 132

[9] Xu Z, Rahman MF. Direct torque and flux regulation of an IPM synchronous motor drive using variable structure control approach. IEEE Transactions on Power Electronics. 2007;22(6):2487–2498. 132

[10] Foo G, Rahman M. Direct torque and flux control of an IPM synchronous motor drive using a backstepping approach. IET electric power applications. 2009;3(5):413–421. 132

[11] Uddin MN, Radwan TS, Rahman MA. Performance of interior permanent magnet motor drive over wide speed range. IEEE Transactions on Energy Conversion. 2002;17(1):79–84. 132

[12] Najjar-Khodabakhsh A, Soltani J. MTPA control of mechanical sensorless IPMSM based on adaptive nonlinear control. ISA transactions. 2016;61:348–356. 132, 134

[13] Ichikawa S, Tomita M, Doki S, Okuma S. Sensorless control of permanent-magnet synchronous motors using online parameter identification based on system identification theory. IEEE Transactions on Industrial Electronics. 2006;53(2):363–372. 132

[14] Bolognani S, Tubiana L, Zigliotto M. Extended Kalman filter tuning in sensorless PMSM drives. IEEE Transactions on Industry Applications. 2003;39(6):1741–1747. 132

[15] Bolognani S, Tubiana L, Zigliotto M. EKF-based sensorless IPM synchronous motor drive for flux-weakening applications. IEEE Transactions on Industry Applications. 2003;39(3):768–775. 132

[16] Shi Y, Sun K, Huang L, Li Y. Online identification of permanent magnet flux based on extended Kalman filter for IPMSM drive with position sensorless control. IEEE Transactions on Industrial Electronics. 2011;59(11):4169–4178. 132

[17] Mohamed YR, Lee TK. Adaptive self-tuning MTPA vector controller for IPMSM drive system. IEEE Transactions on Energy Conversion. 2006;21(3):636–644. 132

[18] Wang G, Li Z, Zhang G, Yu Y, Xu D. Quadrature PLL-based high-order sliding-mode observer for IPMSM sensorless control with online MTPA control strategy. IEEE Transactions on Energy Conversion. 2012;28(1):214–224. 132

[19] Uddin MN, Rebeiro RS. Online efficiency optimization of a fuzzy-logic-controller-based IPMSM drive. IEEE Transactions on Industry Applications. 2010;47(2):1043–1050. 132

[20] Jung SY, Hong J, Nam K. Current minimizing torque control of the IPMSM using Ferrari's method. IEEE Transactions on Power Electronics. 2013;28(12):5603–5617. 132

[21] Andreescu GD, Pitic CI, Blaabjerg F, Boldea I. Combined flux observer with signal injection enhancement for wide speed range sensorless direct torque control of IPMSM drives. IEEE Transactions on energy conversion. 2008;23(2):393–402. 132

[22] Qiu X, Huang W, Bu F, Hu Y. Virtual Hall method for sensorless control of IPMSMs using high-frequency signal injection. Electronics letters. 2013;49(17):1092–1094. 132

[23] Chen Z, Tomita M, Doki S, Okuma S. An extended electromotive force model for sensorless control of interior permanent-magnet synchronous motors. IEEE transactions on Industrial Electronics. 2003;50(2):288–295. 133

[24] Zarchi HA, Soltani J, Markadeh GA. Adaptive input–output feedback-linearization-based torque control of synchronous reluctance motor without mechanical sensor. IEEE Transactions on Industrial Electronics. 2009;57(1):375–384. 133, 134, 136

[25] Moradian M, Soltani J, Benbouzid M, Najjar-Khodabakhsh A. A Parameter Independent Stator Current Space-Vector Reference Frame-Based Sensorless IPMSM Drive Using Sliding Mode Control. Energies. 2021;14(9):2365. 133

[26] Fazeli S, Ping H, Zarchi HA, Soltani J. Robust maximum torque per ampere (MTPA) control of interior permanent magnet synchronous motor drives using adaptive input-output feedback linearization approach. In: 2009 International Conference for Technical Postgraduates (TECHPOS). IEEE; 2009. p. 1–6. 133

[27] Vas P. Sensorless vector and direct torque control. Oxford university press google schola. 1998;2:265–273. 133

[28] Moradian M, Soltani J, Najjar-Khodabakhsh A, Markadeh GA. Adaptive torque and flux control of sensorless IPMSM drive in the stator flux field oriented reference frame. IEEE Transactions on Industrial Informatics. 2018;15(1):205–212. 133

[29] Khalil HK. Nonlinear Systems. Prentice Hall; 1996. 134

[30] Zarchi HA, Markadeh GRA, Soltani J. Direct torque and flux regulation of synchronous reluctance motor drives based on input–output feedback linearization. Energy Conversion and Management. 2010;51(1):71–80. 135

[31] Van Der Broeck HW, Skudelny HC, Stanke GV. Analysis and realization of a pulsewidth modulator based on voltage space vectors. IEEE transactions on industry applications. 1988;24(1):142–150. 136